LUND UNIVERSITY

Enzyme dynamics during catalysis

Eisenmesser, Elan Zohar; Bosco, Daryl A; Akke, Mikael; Kern, Dorothee

Link to publication

Total number of authors:
4

Data (i) had to have small variance (as gauged by reported SE) and (ii) had to be reported in units of kg of dry weight per plant. A total of 385 species are represented in the complete data set (including arborescent monocots, dicots, and conifers). Data for the intraspecific scaling of plant organ biomass were collected by B.J.E. primarily from the agricultural and forestry literature (25, 27, 28).

21. M_L, M_S, and M_R were each computed for an average plant from each community or experimental manipulation with the quotient of total plant biomass per site or treatment and plant density. Model type II (reduced major axis) regression analyses were then used to determine scaling exponents and allometric constants (regression slopes and y intercepts designated as α_{RMA} and β_{RMA}, respectively), because functional rather than predictive relation were sought among variables that were biologically interdependent and subject to unknown measurement error (7). Because many authors failed to report all of the necessary parameters required to assess M_L, M_S, and M_R, the sample size of regression analyses varies across statistical comparisons.
22. Supplementary materials can be found on *Science* Online at www.sciencemag.org/cgi/content/full/295/5559/1517/DC1.
23. F. A. Bazzaz, in *Plant Resource Allocation*, F. A. Bazzaz, J. Grace, Eds. (Academic Press, New York, 1997), pp. 1–37.
24. R. M. Callaway, E. H. DeLucia, W. H. Schlesinger, *Ecology* **75**, 147 (1994).
25. W. B. Smith, *Allometric biomass equations for 98 species of herbs, shrubs, and small trees* (North Central Forest Experimental Station Research Note NC-299, Forest Service U.S. Department of Agriculture, Washington, DC, 1983).
26. B. J. Enquist, K. J. Niklas, *Nature* **410**, 655 (2001).
27. W. H. Pearsall, *Ann. Bot.* **41**, 549 (1927).
28. C. Monk, *Bull. Torrey Bot. Club* **93**, 402.20 (1966).
29. We thank E. Charnov, A. Ellison, D. Ackerly, H.-C. Spatz, L. Sack, and D. Raup for discussions or comments on earlier drafts of this manuscript. This work stems as an outgrowth of discussions from the Body Size in Ecology and Evolution Working Group (F. A. Smith, principle investigator) sponsored by The National Center for Ecological Analysis and Synthesis. B.J.E. was supported by NSF; K.J.N. was supported by an Alexander von Humboldt Forschungspreis and New York State Hatch grant funds.

Enzyme Dynamics During Catalysis

Elan Zohar Eisenmesser,[1] Daryl A. Bosco,[1] Mikael Akke,[2] Dorothee Kern[1]*

Internal protein dynamics are intimately connected to enzymatic catalysis. However, enzyme motions linked to substrate turnover remain largely unknown. We have studied dynamics of an enzyme during catalysis at atomic resolution using nuclear magnetic resonance relaxation methods. During catalytic action of the enzyme cyclophilin A, we detect conformational fluctuations of the active site that occur on a time scale of hundreds of microseconds. The rates of conformational dynamics of the enzyme strongly correlate with the microscopic rates of substrate turnover. The present results, together with available structural data, allow a prediction of the reaction trajectory.

Although classical enzymology together with structural biology have provided profound insights into the chemical mechanisms of many enzymes (1), enzyme dynamics and their relation to catalytic function remain poorly characterized. Because many enzymatic reactions occur on time scales of micro- to milliseconds, it is anticipated that the conformational dynamics of the enzyme on these time scales might be linked to its catalytic action (2). Classically, enzyme reactions are studied by detecting substrate turnover. Here, we examine enzyme catalysis in a nonclassical way by characterizing motions in the enzyme during substrate turnover. Dynamics of enzymes during catalysis have previously been detected with methods such as fluorescent resonance energy transfer, atomic force microscopy, and stopped-flow fluorescence, which report on global motions of the enzyme or dynamics of particular molecular sites. In contrast, nuclear magnetic resonance (NMR) spectroscopy enables investigations of motions at many atomic sites simultaneously (3, 4). Previous NMR studies reporting on the time sca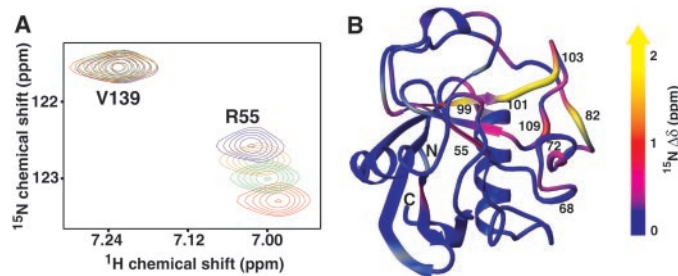les, amplitudes, and energetics of motions in proteins, have provided information on the relation between protein mobility and function (5–15). Here, we have used NMR relaxation experiments to advance these efforts by characterizing conformational exchange in an enzyme, human cyclophilin A (CypA), during catalysis.

CypA is a member of the highly conserved family of cyclophilins that are found in high concentrations in many tissues. Cyclophilins are peptidyl-prolyl cis/trans isomerases that catalyze the interconversion between cis and trans conformations of X-Pro peptide bonds, where "X" denotes any amino acid. CypA operates in numerous biological processes (16, 17). It is the receptor for the immunosuppressive drug cyclosporin A, is essential for HIV infectivity, and accelerates protein folding in vitro by catalyzing the rate-limiting cis/trans isomerization of prolyl peptide bonds (18, 19). However, its function in vivo and its molecular mechanism are still in dispute. X-ray structures of CypA in complex with different peptide ligands show cis X-Pro bonds (20, 21), except for a trans conformation in the CypA/HIV-1 capsid complex (22, 23). In each case, only one conformer was observed in the crystal, even though both isomers must bind to CypA for catalysis of cis/trans isomerization to occur.

We characterized motions in CypA during catalysis with the use of ^{15}N spin relaxation experiments with and without the substrate Suc-Ala-Phe-Pro-Phe-4-NA (24). Longitudinal (R_1) and transverse (R_2) auto-relaxation rates, transverse cross-correlated cross-relaxation rates (η_{xy}), and {^1H}-^{15}N nuclear Overhauser enhancements (NOE) were measured for all backbone amides in CypA (25). Though all parameters are sensitive to "fast" motions (pico- to nanoseconds), only R_2 is sensitive to "slow" conformational exchange (micro- to milliseconds) (5–8). A progressive substrate-induced shift for several CypA amide resonances (Fig. 1) indicates catalysis-linked motions. It shows (i) that these amides experience different magnetic environments in free CypA (E) and in CypA bound to substrate (ES) and (ii) that the

[1]Department of Biochemistry, Brandeis University, Waltham, MA 02454, USA. [2]Department of Biophysical Chemistry, Lund University, Post Office Box 124, SE-221 00 Lund, Sweden.

*To whom correspondence should be addressed. E-mail: dkern@brandeis.edu

Fig. 1. Chemical shift changes of the amide signals in CypA upon titration with the substrate Suc-Ala-Phe-Pro-Phe-4-NA. (**A**) At a constant CypA concentration of 0.43 mM, spectra were recorded at 0 mM (blue), 0.38 mM (orange), 1.01 mM (green), and 2.86 mM (red) substrate. The signal of R55 is progressively shifting upon addition of increasing amounts of substrate, indicating fast conformational exchange during catalysis. The observed chemical shifts are population-weighted averages of E and ES, and thus shift towards the position of the ES complex with increasing amounts of substrate. In contrast, the signal of V139 is not affected by catalysis. (**B**) The chemical shift differences between free CypA and in the presence of 2.86 mM substrate were mapped onto the structure (1RMH) (21) with the use of a continuous color scale.

exchange rates between these states are faster than the difference in their frequencies, i.e., the time scale of exchange falls in the range of 10^{-5} to 10^{-3} s. In the presence of substrate, at least three different states of CypA exist in equilibrium (Scheme 1). Exchange between these will increase the value of R_2 by an amount R_{ex} above that observed in free CypA, provided that the nuclear spin experiences different chemical shifts in at least two of the three states (8). Direct measurements of R_2 revealed that during catalysis CypA undergoes microsecond conformational exchange in specific regions of the protein. A significant increase in R_2 was observed for 10 out of 160 backbone amide nitrogens (26) (Figs. 2 and 3), which together define a contiguous region in the structure (Fig. 3). The measured R_{ex} for a particular amide does not necessarily indicate motion of that amide itself. R_{ex} can be caused by slow time scale motions of nearby atoms. Addition of substrate induces only minor changes in pico- to nanosecond dynamics, as evidenced by R_1, η_{xy}, and $\{^1H\}$-^{15}N NOE (27). Thus, measure-ment of R_2 identifies "hot spots" of micro- to millisecond dynamics associated with either or both of the processes involved in catalysis: binding and isomerization.

Can the microscopic reaction steps be separated? The minimal reaction scheme (Scheme 1) consists of three microscopic reaction steps: binding of (i) cis and (ii) trans isomers and (iii) the catalytic step of substrate isomerization on the enzyme. We separated the effects of binding and isomerization by monitoring changes in R_2 as a function of substrate concentration. The relative contributions to R_2 from exchange due to binding and isomerization have different dependencies on the total substrate concentration. For most residues, R_2 first increases and then decreases with the addition of substrate (Fig. 2, D and E, and Fig. 4A). This pattern of maximum chemical exchange at intermediate substrate concentrations—where E, ES_{cis}, and ES_{trans} are all significantly populated—is diagnostic of a predominant effect due to binding (see Eq. 1). In contrast, R_2 increases monotonically with substrate concentration for R55 (28) (Figs.

2B and 4B). This increase in R_2 with a concomitant increase in populations of ES_{cis} and ES_{trans} pinpoints a significant conformational exchange contribution to R_2 from interconversion between ES_{cis} and ES_{trans}.

Do the exchange dynamics observed for the enzyme correspond to the microscopic catalytic steps of substrate turnover? To shed light on this fundamental question, we determined rate constants for the conformational changes on the enzyme and compared them with rate constants of substrate interconversion. For residues that report only on binding, a simple two-state exchange model (including the free and a single bound state) can be applied, enabling the use of closed analytical formulae to determine the binding constant, off-rate, and chemical shifts. The exchange contribution (R_{ex}) to R_2 may be approximated as (29):

$$R_{ex} = P_E P_{ES} \frac{\delta\omega^2}{k_{ex}} \left(1 - \frac{2}{k_{ex}\tau_{cp}} \tanh\left[\frac{k_{ex}\tau_{cp}}{2} \right] \right) \quad (1)$$

where P_E and P_{ES} are the fractional populations of the free (E) and bound (ES) states, $\delta\omega$ is the chemical shift difference between E and ES, k_{ex} is the exchange rate, and τ_{cp} is the delay between refocusing pulses in the Carr-Purcell-Meiboom-Gill (CPMG) experiment. Expressing Eq. 1 in terms of the free substrate concentration, $[S_F]$, and an effective dissociation constant, $K_D^{obs} = P_E[S_F]/P_{ES} = k_{off}/k_{on}$, and making the substitution $k_{ex} = k_{off} + k_{on}[S_F] = k_{off}(1 + [S_F]/K_D^{obs}) = k_{off}\psi$, one gets

$$R_{ex} = \frac{\delta\omega^2}{k_{off}\psi^3} \frac{[S_F]}{K_D^{obs}} \left(1 - \frac{2}{k_{off}\psi\tau_{cp}} \tanh\left[\frac{k_{off}\psi\tau_{cp}}{2} \right] \right) \quad (2)$$

where $[S_F]$ is a function of K_D^{obs} and the total concentrations of substrate and enzyme, k_{off} is the off-rate, and k_{on} is the on-rate (30). Hence, K_D^{obs}, k_{off}, and $\delta\omega$ can be estimated by nonlinear regression (31). The data for residues K82, L98, N102, and A103 are fit well by the two-state model, yielding values of K_D^{obs} between 0.95 and 1.20 mM, and values of k_{off} between 10,700 and 14,800 s^{-1} (Fig. 4A). These values agree within uncertainties with those measured from line shape analysis of the substrate (32). Next, we obtained quantitative estimates of the rate constants of protein dynamics by simulating the R_2 rates for the full three-state model of Scheme 1. Excellent agreement between the simulated and experimental data was obtained with the use of the rate constants of cis/trans isomerization determined separately from line shape analysis (32) together with reasonable chemical shift differences between the three states (33) (Fig. 4). The results confirm the qualitative evaluation of R_2 outlined above: for

Scheme 1. Three-state model of CypA catalysis. E is the free enzyme, and ES_{cis} and ES_{trans} are the two Michaelis-Menten complexes with the substrate in the cis and trans conformations, respectively. K_D is the dissociation constant, k_{off} the off-rate, k_{on} the on-rate, k_{cat}^{ct} and k_{cat}^{tc} are the rate constants of isomerization. Superscripts cis and trans identify the cis and trans isomer, respectively. CypA catalyzes the cis/trans isomerization of the Phe-Pro peptide bond of the substrate used here with a turnover rate of several thousands per second (43, 46).
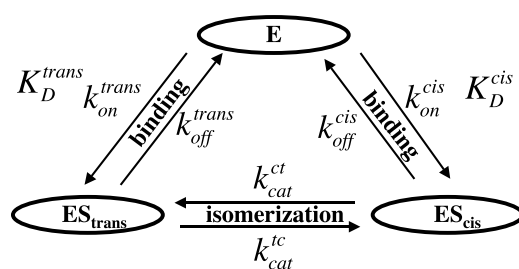
Fig. 2. Comparison of backbone ^{15}N R_2 relaxation between free CypA and CypA during catalysis. (**A**) R_2 rate constants of CypA are shown for samples with 0 mM (dark blue), 1.01 mM (green), and 2.86 mM substrate (red). Four regions exhibiting changes in R_2 due to steady-state turnover are circled and are expanded in (**B** to **E**), which include also data for samples with 0.04 mM (light blue), 0.08 mM (magenta), and 0.45 mM substrate (gold).
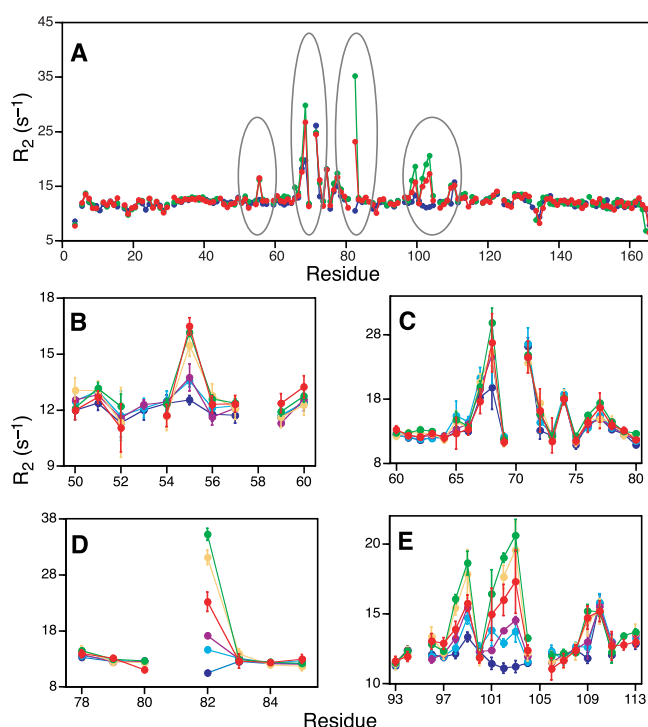
most residues the binding processes dominate the exchange contribution, whereas for others a contribution from the isomerization step is required to yield satisfactory fits.

The backbone amide nitrogen of R55 clearly experiences conformational exchange associated with the isomerization and binding process. Because the backbone amide group is distant from the substrate binding site, it is unlikely that the observed exchange merely reflects a conformational change of the bound peptide in a rigid active site. Rather, the results provide evidence for conformational fluctuations in the enzyme. Notably, R55 is essential for catalysis (34). Its side-chain guanidino group is hydrogen bonded to the prolyl nitrogen of the substrate, and, thus, promotes isomerization by weakening the double-bond character of that peptide bond (20, 21, 23, 34). The good agreement between the ^{15}N relaxation results and those from substrate line enzyme shape analysis implies that the observed conformational dynamics of the enzyme are strongly and quantitatively correlated with the chemical steps of substrate interconversion. Furthermore, the conformational fluctuations of the enzyme are likely to be collective motions, because

similar rate constants were inferred for several backbone amides.

Interpretation of the results in light of structural data provides additional insights into CypA catalysis. We focus here on residues that show conformational exchange dynamics only during catalysis, thus excluding the loop from residues 68–77 that also undergoes conformational exchange in resting CypA (35). Several residues (101–103 and 109) with catalysis-linked exchange are physically close to the substrate bound in cis (Fig. 3A) (36). However, L98 and S99 are distant from the peptide in the cis conformation, yet undergo exchange during the catalytic cycle and show chemical shift changes upon titration with substrate that are comparable to those observed for residues 101–103 and 109 (Figs. 1 and 3). Though the structure of the enzyme in complex with the corresponding trans isomer of the peptide is not known, our results suggest that L98 and S99 may be interacting with the trans peptide. Thus, we propose a reaction trajectory that involves a rotation of the COOH-terminal peptide segment around the prolyl peptide bond while the NH$_2$-terminal part remains bound to the enzyme (37). This conformational rearrangement brings

all residues exhibiting exchange, except R55, T68, and K82, into close proximity with the peptide (Fig. 3B). K82 is located within a loop remote from the active site (21). Our relaxation data clearly indicate the involvement of K82 in substrate binding, as confirmed by a reduction in substrate affinity for the mutant Lys^{82} → Ala^{82} (K82A) (38). As shown in Fig. 1B, additional backbone amides show chemical shift changes during turnover. However, these changes are smaller than those observed for the aforementioned residues; hence, their exchange contribution to R_2 is below the present detection limit (Eq. 1).

Taking all results together, we can envision the enzymatic cycle of CypA as follows (Scheme 1 and Fig. 3): the substrate exists in the cis and trans conformations free in solution. Both isomers can bind to CypA. For the cis isomer, the areas around 101–103, 109, 82, and 55 are important in the binding process, which is close to diffusion-controlled. After binding, the enzyme catalyzes a rotation of the prolyl peptide bond by 180°. For this to occur, the substrate tail COOH-terminal to proline likely swings around to contact the area around residues 98 and 99 (Fig. 3), whereas the NH$_2$-terminal tail of the substrate stays fixed. In other words, the enzyme holds on to the substrate through this binding interaction. The isomerization step takes place with a rate constant of about 9000 s^{-1}, and motions of the protein coincide with the rate of substrate rotation. The major player in catalysis is R55, for which the observed changes in backbone conformation are likely to be coupled with motions of the catalytically essential side chain. After the isomerization step, the enzyme releases the substrate, which is now in trans, with a rate constant of about 13,000 s^{-1}.

The approach outlined here allows the identification of the dynamic "hot spots" during catalysis and reveals that the time scales of protein dynamics coincide with that of substrate turnover. However, it does not provide a detailed physical picture of the motions during catalysis. To do this, side-chain dynamics need to be included and, ultimately, all the relaxation data need to be used in molecular dynamics calculations. The application of relaxation measurements during substrate turnover promises to be of general use in understanding the dynamic behavior of enzymes and its relation to catalysis.

Fig. 3. Residues in CypA exhibiting microsecond time scale dynamics during catalysis. (**A**) Structure of the cis conformation of the substrate Suc-Ala-Phe-Pro-Phe-4-NA (green) bound to CypA, based on the x-ray structure of CypA complexed with the cis form of Suc-Ala-Ala-Pro-Phe-4-NA (1RMH) (21). CypA residues with chemical exchange in both the presence and absence of substrate are color coded in blue (F67, N71, G74, S77, and S110). Residues in red exhibit chemical exchange only during turnover (R55, K82, L98, S99, A101, N102, A103, and G109). Residues shown in magenta exhibit chemical exchange in the absence of substrate, but increase in its presence (T68 and G72). (**B**) Suggested trajectory of the enzymatic pathway based on the dynamics results. CypA catalyzes prolyl isomerization by rotating the part COOH-terminal to the prolyl peptide bond by 180° to produce the trans conformation of the substrate. In this model, the observed exchange dynamics for residues in strand 5 can be explained.
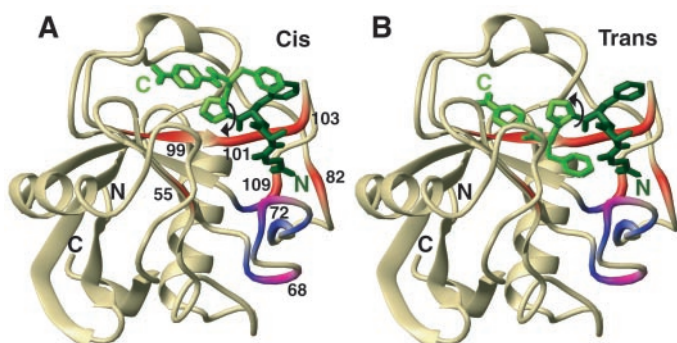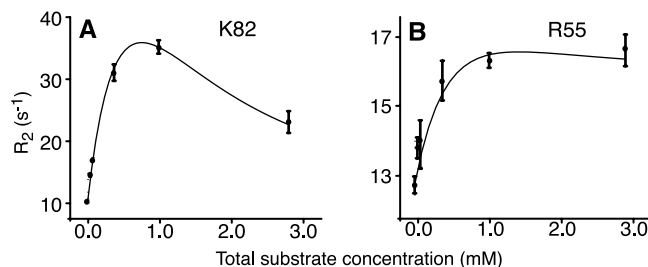

Fig. 4. Quantification of exchange dynamics in CypA during catalysis. R_2 rate constants are plotted as a function of total substrate concentration. (**A**) R_2 data for K82. The continuous line indicates the fitted Eq. 2, including contributions only from binding. K_D^{obs} = 1.18 mM; k_{off} = 11,100 s^{-1}; $\delta\omega$ = 1450 s^{-1} (3.8 ppm). (**B**) R_2 data for R55. The continuous line indicates a fit according to the full three-state model, including contributions from both binding and isomerization (32); using K_D^{obs} = 1.19 mM, then k_{off}^{trans} = 13,000 s^{-1}; k_{off}^{cis} = 10,000; k_{cat}^{ct} = 9000s^{-1}; k_{cat}^{ct} = 5100 s^{-1}; $\delta\omega$ = 440 s^{-1} [1.2 parts per million (ppm)]; $\delta\omega_{ct}$ = 640 s^{-1} (1.7 ppm). Of these parameters, only $\delta\omega_{ct}$ and $\delta\omega_{Et}$ were determined de novo, whereas for the others approximate values were known from the two-site fitting and from line shape analysis.

References and Notes
1. T. C. Bruice, S. J. Benkovic, *Biochemistry* **39**, 6267 (2000).
2. A. Fersht, *Structure and Mechanism in Protein Science. A Guide to Enzyme Catalysis and Protein Folding* (Freeman, New York, ed. 1, 1999) pp. 44–51.
3. M. W. F. Fischer, A. Majumdar, E. R. P. Zuiderweg, *Progr. Nucl. Magn. Reson. Spectrosc.* **33**, 207 (1998).
4. A. G. Palmer, 3rd, *Curr. Opin. Struct. Biol.* **7**, 732 (1997).
5. R. Ishima, D. A. Torchia, *Nature Struct. Biol.* **7**, 740 (2000).
6. O. Jardetzky, *Prog. Biophys. Mol. Biol.* **65**, 171 (1996).
7. L. E. Kay, *Nature Struct. Biol.* **5** (suppl.), 513 (1998).

8. A. G. Palmer, C. D. Kroenke, J. P. Loria, *Methods Enzymol.* **339**, 204 (2001).

9. L. K. Nicholson *et al.*, *Nature Struct. Biol.* **2**, 274 (1995).

10. J. C. Williams, A. E. McDermott, *Biochemistry* **34**, 8309 (1995).

11. R. Ishima, D. I. Freedberg, Y. X. Wang, J. M. Louis, D. A. Torchia, *Struct. Fold Des.* **7**, 1047 (1999).

12. L. Wang *et al.*, *Proc. Natl. Acad. Sci. U.S.A.* **98**, 7684 (2001).

13. S. Rozovsky, G. Jogl, L. Tong, A. E. McDermott, *J. Mol. Biol.* **310**, 271 (2001).

14. M. J. Osborne, J. Schnell, S. J. Benkovic, H. J. Dyson, P. E. Wright, *Biochemistry* **40**, 9846 (2001).

15. S. Y. Stevens, S. Sanker, C. Kent, E. R. Zuiderweg, *Nature Struct. Biol.* **8**, 947 (2001).

16. S. F. Gothel, M. A. Marahiel, *Cell Mol. Life Sci.* **55**, 423 (1999).

17. P. Rovira, L. Mascarell, P. Truffa-Bachi, *Curr. Med. Chem.* **7**, 673 (2000).

18. S. F. Gothel, M. Herrler, M. A. Marahiel, *Biochemistry* **35**, 3636 (1996).

19. C. Schiene, G. Fischer, *Curr. Opin. Struct. Biol.* **10**, 40 (2000).

20. Y. Zhao, H. Ke, *Biochemistry* **35**, 7362 (1996).

21. ———, *Biochemistry* **35**, 7356 (1996).

22. T. R. Gamble *et al.*, *Cell* **87**, 1285 (1996).

23. Y. Zhao, Y. Chen, M. Schutkowski, G. Fischer, H. Ke, *Structure* **5**, 139 (1997).

24. The plasmid containing the gene for human CypA was a generous gift from W. Sundquist. CypA was expressed in BL21/DE3 cells in ^{15}N-labeled minimal media. Cells were lysed in 25 mM MES, pH 6.1 and 5 mM β-mercaptoethanol and were purified on a S-Sepharose column equilibrated with the same buffer. Remaining DNA was removed on a Q-Sepharose column with 50 mM Tris, pH 7.8 and 5 mM β-mercaptoethanol. NMR sample conditions were 0.43 mM CypA in 50 mM sodium phosphate buffer, pH 6.5, 3 mM dithiothreitol (DTT), 10% D_2O, with peptide concentrations between 0.04 and 2.6 mM. CypA retained full activity during NMR data collection as determined by the coupled chymotrypsin assay (*39*), performed on samples before and after each series of relaxation experiments.

25. Spectra were collected on Varian INOVA 600 spectrometers (Varian, Palo Alto, CA) at 25 ± 0.1°C. ^{1}H-^{15}N heteronuclear single-quantum correlation (HSQC) spectra were acquired with the use of WATERGATE (*40*). ^{15}N R_1, R_2, {^{1}H}-^{15}N NOE, and η_{xy} experiments were performed using pulse sequences reported previously (*41, 42*). For each sample, at least seven R_1 delays and eight R_2 delays were acquired, ranging from 100 to 1000 ms and from 10 to 150 ms, respectively. At least four relaxation delays were acquired for the η_{xy} measurement, ranging from 30 to 120 ms. Spectra were acquired with 2048 and 128 complex points in the ^{1}H and ^{15}N dimensions, respectively. Processing and analysis of the NMR spectra were performed with the use of Felix (Accelrys, San Diego, CA). Uncertainties in peak heights were estimated from duplicate spectra. Relaxation rates were determined using the program CurveFit (A. G. Palmer).

26. Additional residues show signs of exchange if the CPMG pulse train is substituted for a single refocusing pulse (*12*).

27. With addition of the peptide, several residues, including residues N102 and A103, exhibit a decrease in R_1, whereas no significant change is observed for the {^{1}H}-^{15}N NOE (see the supplementary material for the complete R_1 and {^{1}H}-^{15}N NOE data, available on *Science* Online at www.sciencemag.org/cgi/content/full/295/5559/1520/DC1). Thus, for these residues, pico- to nanosecond motions are more restricted in the presence of peptide. A reduction in mobility on this time scale has also been observed for residues 101–104 in the presence of the inhibitor cyclosporin A (*35*).

28. Single-letter abbreviations for the amino acid residues are as follows: A, Ala; C, Cys; D, Asp; E, Glu; F, Phe; G, Gly; H, His; I, Ile; K, Lys; L, Leu; M, Met; N, Asn; P, Pro; Q, Gln; R, Arg; S, Ser; T, Thr; V, Val; W, Trp; and Y, Tyr.

29. Z. Luz, S. Meiboom, *J. Chem. Phys.* **39**, 366 (1963).

30. $[S_F] = (\sqrt{(K_D^{obs} - [S_T] + [E_T])^2 + 4[S_T]K_D^{obs}} - (K_D^{obs} - [S_T] + [E_T]))/2$, where $[S_T]$ and $[E_T]$ are the total concentrations of substrate and enzyme, respectively.

31. We first evaluated Eq. 2 in the limit $k_{ex} \gg \tau_{cp}$, which amounts to fitting K_D^{obs} and $\delta\omega^2/k_{off}$. This yields a good estimate of K_D^{obs} (accurate to within approximately 10%), but a poorer estimate of $\delta\omega^2/k_{off}$ (accurate to within approximately 25%). Knowledge of K_D^{obs} affords calculation of $\delta\omega$ from the relation $\omega_{obs} = p_{ES}\delta\omega + \omega_E$, where ω_{obs} and ω_E are the chemical shifts observed at a given concentration of substrate and in free CypA, respectively. Note that from the estimated K_D^{obs} of 1.1 mM, p_{ES} is calculated to 0.67 for the highest substrate concentration used. Subsequently, k_{off} was estimated by fitting the full Eq. 2 while keeping $\delta\omega$ fixed. This approach circumvents problems that may otherwise arise when optimizing the individual parameters k_{off} and $\delta\omega$, which appear as a ratio in Eq. 2, simultaneously.

32. Line shape analysis was performed on the peptide in the presence of catalytic amounts of CypA at 25°C with the use of the method described (*43*) to determine the microscopic rate constants of catalysis.

33. The Bloch-McConnell equations (*44*) describing the transverse relaxation in the full three-state system (Scheme 1) were integrated numerically with the use of Mathematica 4.0 (Wolfram Research, Champaign, IL), and monoexponential decays were fitted to the resulting data sets, yielding transverse relaxation rates for each residue at each concentration of substrate. The three-state system is underdetermined by the present number of experimental data points. However, starting from parameter values determined separately from line shape analysis of the substrate during catalysis and from the two-site fitting, a sensitivity analysis of the parameter space yields ranges of possible values for the rate constants. The chemical shift differences between the three states were adjusted but kept within a reasonable range. The chemical shift differences between the free and bound states are related to the maximum chemical shift change ($\delta\omega$) observed upon substrate addition and were determined separately by: $\delta\omega = \delta\omega_{ct}/(1 + K_{eq}) - \delta\omega_{Et}$. $K_{eq} = [ES_{cis}]/[ES_{trans}]$ is obtained from line shape analysis, $\delta\omega_{ct}$ is the chemical shift difference between ES_{cis} and ES_{trans}, and $\delta\omega_{Et}$ is the chemical shift difference between E and ES_{trans}.

34. L. D. Zydowsky *et al.*, *Protein Sci.* **1**, 1092 (1992).

35. M. Ottiger, O. Zerbe, P. Guntert, K. Wuthrich, *J. Mol. Biol.* **272**, 64 (1997).

36. An initial structural model of CypA in complex with Suc-Ala-Phe-Pro-Phe-4-NA was built from the crystal structure of CypA in complex with the similar peptide Suc-Ala-Ala-Pro-Phe-4-NA in the cis conformation (PDB entry 1RMH) (*21*). All structures were viewed and built using MOLMOL (*45*).

37. Chemical shift changes for this substrate upon binding to cyclophilin have previously been calculated by line shape analysis, and these data also support the proposed model for the conformational change (*43*).

38. D. Kern, unpublished data.

39. G. Fischer, H. Bang, C. Mech, *Biomed. Biochim. Acta* **43**, 1101 (1984).

40. M. Piotto, V. Saudek, V. Sklenar, *J. Biomol. Nucl. Magn. Reson.* **2**, 661 (1992).

41. N. A. Farrow *et al.*, *Biochemistry* **33**, 5984 (1994).

42. N. Tjandra, A. Szabo, A. Bax, *J. Am. Chem. Soc.* **118**, 6986 (1996).

43. D. Kern, G. Kern, G. Scherer, G. Fischer, T. Drakenberg, *Biochemistry* **34**, 13594 (1995).

44. H. M. McConnell, *J. Chem. Phys.* **28**, 430 (1958).

45. R. Koradi, M. Billeter, K. Wuthrich, *J. Mol. Graph.* **14**, 51 (1996).

46. The microscopic rate constants of substrate interconversion were determined separately from line shape analysis of the peptide NMR spectrum using previously established methods (*43*).

47. We are grateful to C. Miller for assistance with the quantitative analysis. Supported by NIH grant GM62117 (D.K.) and VR grants K-650-19981661 and S-614-989 (M.A.). Instrumentation grants were awarded by the NSF and the Keck foundation to (D.K.) and by the Knut and Alice Wallenberg foundation (M.A.).

Role of Nucleoporin Induction in Releasing an mRNA Nuclear Export Block

Jost Enninga,[1] David E. Levy,[2] Günter Blobel,[1]* Beatriz M. A. Fontoura[1,3]

Signal-mediated nuclear import and export proceed through the nuclear pore complex (NPC). Some NPC components, such as the nucleoporins (Nups) Nup98 and Nup96, are also associated with the nuclear interior. Nup98 is a target of the vesicular stomatitis virus (VSV) matrix (M) protein–mediated inhibition of messenger RNA (mRNA) nuclear export. Here, Nup98 and Nup96 were found to be up-regulated by interferon (IFN). M protein–mediated inhibition of mRNA nuclear export was reversed when cells were treated with IFN-γ or transfected with a complementary DNA (cDNA) encoding Nup98 and Nup96. Thus, increased Nup98 and Nup96 expression constitutes an IFN-mediated mechanism that reverses M protein–mediated inhibition of gene expression.

The Nup98 and Nup96 proteins are encoded by a single gene. The primary transcript is alternatively spliced, and the translation products are autocatalytically proteolyzed at one specific site (*1–3*). Nup98 interacts with an intranuclear protein (*4*) and transport factors (*5, 6*). It is involved in nuclear import and export of proteins and RNAs (*7–11*) and is the target of the VSV M protein–mediated inhibition of mRNA export (*12*). A cDNA clone coding for part of the COOH-terminal sequence of Nup96 has been detected among mRNAs that were specifically induced by IFN-γ (*13*).

We found two classical elements, GAS and ISRE, that mediate increased gene expression by IFN (*14, 15*). When U937 cells were incubated with IFN-γ for up to 12